The Effect of the Stiffness of Soft Materials on Hemiwicking Performance

Thomas Germain and Dr. Shawn A. Putnam Mechanical and Aerospace Engineering University of Central Florida, P.O. Box 162993

Orlando, Florida, United States of America, 32816 Email: tmgermain@knights.ucf.edu

ABSTRACT

Fabricating micro and nanosized structures to induce hemiwicking on a heated surface has risen in popularity due to the higher heat flux the surface can experience. Recent studies have focused on the effects on the pillar geometry and spacing on the wicking velocity and the critical heat flux. As a result, a majority of the models that have been derived focus on the fluid properties and the wicking structure geometry and spacing. This study presents changes to the wicking performance when the stiffness of a soft material is taken into effect. Multiple similar wicking structures were fabricated using a negative mold method utilizing an in-house stamping apparatus. Using the mold, multiple polydimethylsiloxane (PDMS) samples were created, where the stiffness of the samples was varied by altering the mixing ratio and the curing time. The wicking velocity of ethanol, isopropyl alcohol, and isooctane did not vary for the samples that had a Young's Modulus greater than 1 MPa, but a notable decrease in the wicking velocity for all three fluids were observed for samples with a Young's Modulus less than 1 MPa. This study provides insight to the importance of the stiffness of the material is for hemiwicking on soft materials and that deformation effects have to be taken into account for Young's Moduli less than 1 MPa.

KEY WORDS: hemiwicking, soft materials, surface wetting, polymer, interfacial dynamics,

NOMENCLATURE

- b width of the sample, m
- D diffusion, m²/s
- d diameter of the pillars, m
- E Young's Modulus, Pa
- F Force, N
- f friction factor, dimensionless
- H height of the pillars, m
- h height of the sample, m
- K structure coefficient, dimensionless
- L Length of the sample, m
- S solid-liquid structure factor, dimensionless
- s distance between pillars, m
- t time, s
- U wicking velocity, m/s
- x distance, m

Greek symbols

- δ displacement (m)
- η pillar array coefficient
- γ surface tension (N/m)

u dynamic viscosity (Pa-s)

Subscripts

eth ethanol

isop isopropyl alcohol

iso isooctane

0 meniscus extension

x x direction

y y direction

INTRODUCTION

Within the study of surface wetting and microfluidics, the phenomenon of hemiwicking has risen in popularity over the past few decades. [1-4] Hemiwicking is the transportation of fluid driven by capillary action through the presence of micro and nano sized hydrophilic structures. [4] These structures have risen in interest due to the ability to transport fluids across a surface without the use of additional moving parts. Heat transfer systems, such as heat pipes, have implemented wicking structures due to the fluid transport and rewetting properties, which increases the overall critical heat flux. [5,6]

Soft material research has also increased in popularity over the past few decades for both research and industry. The microfluidic interactions on soft materials have been investigated due to the necessity of soft materials in multiple areas, including soft tissues, polymer gels, and inkjet printing. [7-9] One main area of research is the deformation that occurs on the surface due to the surface tension of a sessile droplet on a soft surface. Due to the vertical deformations that occur on the soft material, previous wetting models (i.e. Young's Equation) do not accurately describe the wetting behavior of the fluid. [10,11] The changes in the wetting behavior can be

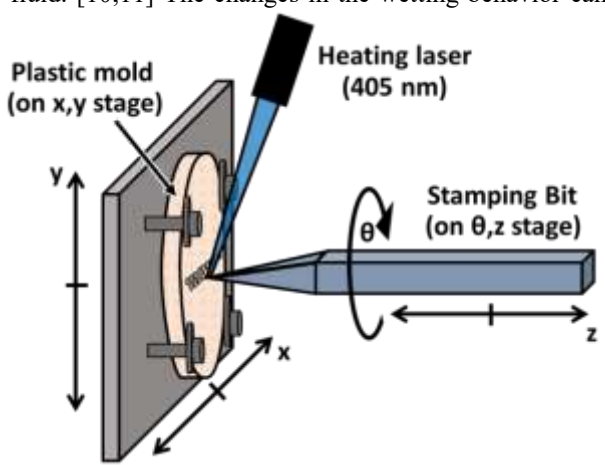


Fig.1 A schematic of the stamping apparatus used to make the negative mold for the PDMS wicking samples [16]

attributed to wrinkling and folding of thin-films cause by the fluid on the surface. [12-13]

This study aims to observe the decrease in wicking performance (i.e. wicking velocity and diffusion) on soft materials compared to previous hemiwicking models. An inhouse stamping apparatus is implemented to fabricate an Acrylic negative mold for the wicking structures. Polydimethylsiloxane (PDMS) of different mixing ratios and different curing times are created to have wicking samples of near identical geometries but varying stiffness. The wicking velocities of ethanol, isopropyl alcohol, and isooctane are then measured to observe any degradation in wicking performance based on the stiffness of the samples. This study will be useful in providing greater understanding for implementing hemiwicking structures in flexible heat pipes which are rising in popularity. [14,15]

RESEARCH METHODS

During this study, three main research methods were implemented. To fabricate the wicking structures, an in-house stamping apparatus was utilized to create a negative mold for the wicking structures. The negative mold is used to create different PDMS samples through a casting method where the stiffnesses of the different samples could be altered. After the samples were created, a cantilevered beam and vertical wicking experiments were conducted to find the Young's Modulus and wicking performance, respectively.

Stamping Apparatus for Sample Fabrication

An in-house stamping apparatus was implemented to create negative molds in a time and cost-effective manner. [16] Figure 1 displays a schematic of the stamping apparatus. Two sets of stepper motors are programmed to operate the stamping apparatus; one set to control the x- and y- position of the acrylic piece and the other to control the z- and θ position of the micro- drill bit. A user created bit map is used to determine the location and depth of the cavities on the acrylic piece. This is used to define the geometry of the pillar array (i.e. S_x , S_y , H). The diameters of the pillars, d, is determined

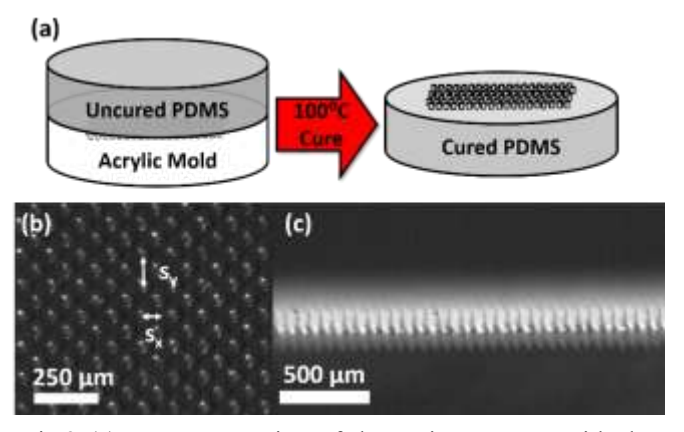


Fig.2 (a) A representation of the curing process with the PDMS once the acrylic mold is obtained. (b) An overhead view of the wicking structures on Sample 2 with the wicking geometry defined. (c) A side image of the pillars on Sample 2

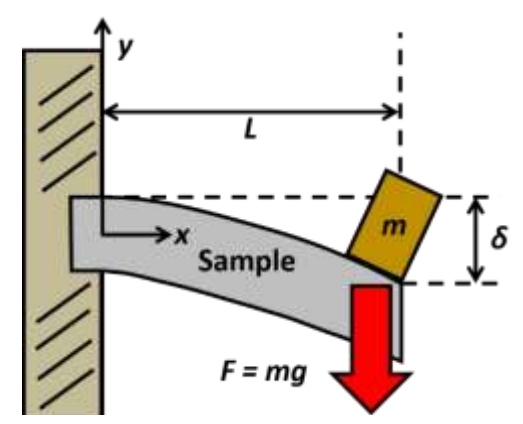


Fig.3 A representation of the cantilevered beam deflection experiments to determine the Young's Modulus of the samples

by the diameter of the micro drill bit used. A heating laser is focus on the micro drill bit to assist the fabrication process.

Once the negative mold is created, uncured PDMS is poured onto the mold. Figure 2(a) displays a schematic for the curing process. For this study, the same mold is used to ensure that the geometry of the pillars will be nearly identical. Table I provides the information regarding the pillar geometries of the samples. The geometric parameters of the camera are found with two cameras with resolutions of 0.176 µm/pixel and 4.14 µm/pixel. To change the stiffness of the different samples, different ratios of the monomer base and cross-linker and different curing times are used to change the stiffness of the samples. Il samples were cured at 1 C. Table II provides the given conditions for each of the samples. [17,18]

Table I: The Wicking Geometry of the Samples Used in This Study

Sample	$s_x(\mu m)$	$s_y(\mu m)$	H (μm)	d (µm)
1	61.6	127.0	120.6	59.0
2	58.4	124.6	123.2	53.1
3	60.3	125.8	160.4	51.3
4	60.8	129.6	120.0	59.2
5	62.5	126.4	121.1	53.8
6	58.2	124.0	123.0	51.5

Cantilevered Beam Experiments

To find the elastic modulus of the wicking structures, a cantilevered beam experiment was implemented, as seen in Figure 3. After the sample was cured and removed from the Acrylic mold, the sample is cut into a rectangle with the pillar array on the sample. A clamp is closed on one side of the sample to create a cantilevered situation. Once clamped, 0.2, 0.5, 1, 2, and 5 g are placed on the end of the sample. The magnitude of the deflection is captured through the use of a flea camera. With the deflection measured, the E of the sample can be calculated through the following relationship:

$$E = \frac{4L^3F}{bh^3\delta} \tag{1}$$

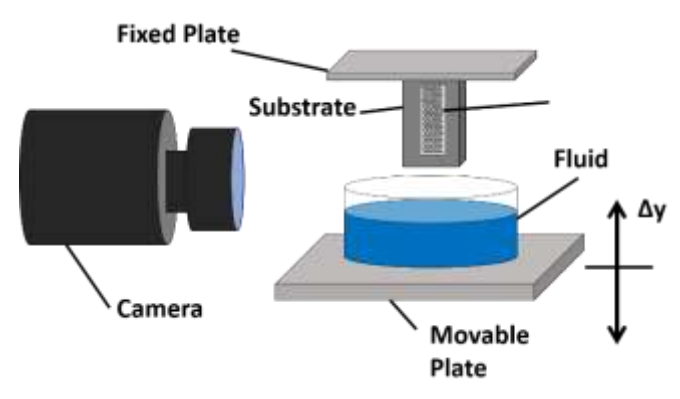


Fig.4 The experimental set up used to induce and measure the wicking velocity with the different working fluids

The stiffness is measured for each of the weights and the average of the stiffness is used for this study. The results from these experiments with the corresponding mixing ratios and curing time are provided in Table II.

Table II: The Stiffness of the PDMS Samples

Sample	Mixing Ratio	Curing Time (Hours)	Young's Modulus (MPa)
1	10:1	1	1.21 ± 0.0910
2	10:1	3	1.16 ± 0.0854
3	15:1	1	0.388 ± 0.134
4	10:1	5	1.95 ± 0.188
5	20:1	1	0.337 ± 0.0443
6	9:1	5	1.98 ± 0.311

Vertical Wicking Experimentation

Figure 4 shows the method used to measure the wicking velocity across the wicking array. Each of the samples were attached above a reservoir of the fluid with a camera (Resolution = 4.14 µm/pixel, frame rate = 0.02 s/frame) focused on the surface of the sample. The three working fluids used for this study are ethanol (γ_{eth} = . 2197 N/m, μ_{eth} = 0.001074 Pa-s), isopropyl alcohol (γ_{isop} = 0.02093 N/m, μ_{isop} = 0.002038 Pa-s), and isooctane (γ_{iso} = . 186 N/m, μ_{iso} = 0.0004784 Pa-s). The sample is then lowered to the reservoir to where the working fluid begins to travel through the array. The motion of the working fluid across the array is captured by the camera, where the videos can be analyzed to measure the wicking velocity and diffusion.

RESULTS & DISCUSSION

The wicking velocity data on the soft material wicking structures are analyzed in two different methods. The first method is comparing the wicking velocity observed to a published wicking model to see the changes in the wicking velocity with the changes in the stiffness of the samples. The second method includes analyzing the change in the diffusion of the three working fluids in the wicking arrays.

Derivation of the Wicking Models

Current models that predict the wicking velocity across an array incorporates the working fluid properties and the pillar geometry in the arrays. Since hemiwicking occurs due to the capillary forces brought upon by the wicking structures, the pillar geometry (i.e. diameter, height) and the pillar spacing are important in designing an array for hemiwicking [19,20]. One common method to define the pillar geometry in an array is the friction factor, f, which is defined as the ratio of the actual surface area to the projected surface area. It can be seen in Figure 2(c) that the pillars on the samples appear to be cylindrical. Therefore, for the pillars in this study, f is defined through the following relationship [19]:

$$f = 1 + \frac{\pi d\sqrt{4h^2 + d^2}}{4s_x s_y} \tag{2}$$

When predicting the wicking velocity through a pillar array, the driving force brought upon by the capillary force and the drag force brought upon by the presence of the pillars need to be taken into account. As the fluid continues to travel across the pillar array, the velocity decreases due to the increase in the overall drag the working fluid is experiencing by the viscous forces. When Kim et al. balances the driving force and the drag force, the following relationship is derived

$$U \sim \frac{\gamma \eta H}{\mu L} \tag{3}$$

where η is defined as

$$\eta = \frac{(s_y - d)(f - 1)}{(s_y - d) + H(f - 1)} \tag{4}$$

Krishnan et al. further studied the wicking velocity but incorporated a structure coefficient, K, to provide a more accurate prediction of wicking velocities for pillar arrays that may yield similar f values but have different geometries. K is defined through the following relationship:

$$K = \left[\frac{Hs_x(s_y - d)(f - 1)^{1/2}}{L} \right]^{1/2}$$
 (5)

Along with K, Krishnan et al. integrated the meniscus extension, x_0 , with the length scale to take into account the various pressures and forces previously not analyzed. Combining K and x_0 yields the solid liquid structure factor, S, which is defined by:

$$S = \frac{K^2}{x_0^2} \tag{6}$$

Based on S and experiments conducted in their study, Krishnan et al. derived a new model for hemiwicking:

$$U = \frac{S}{95\pi} (\frac{\gamma}{\mu}) \tag{7}$$

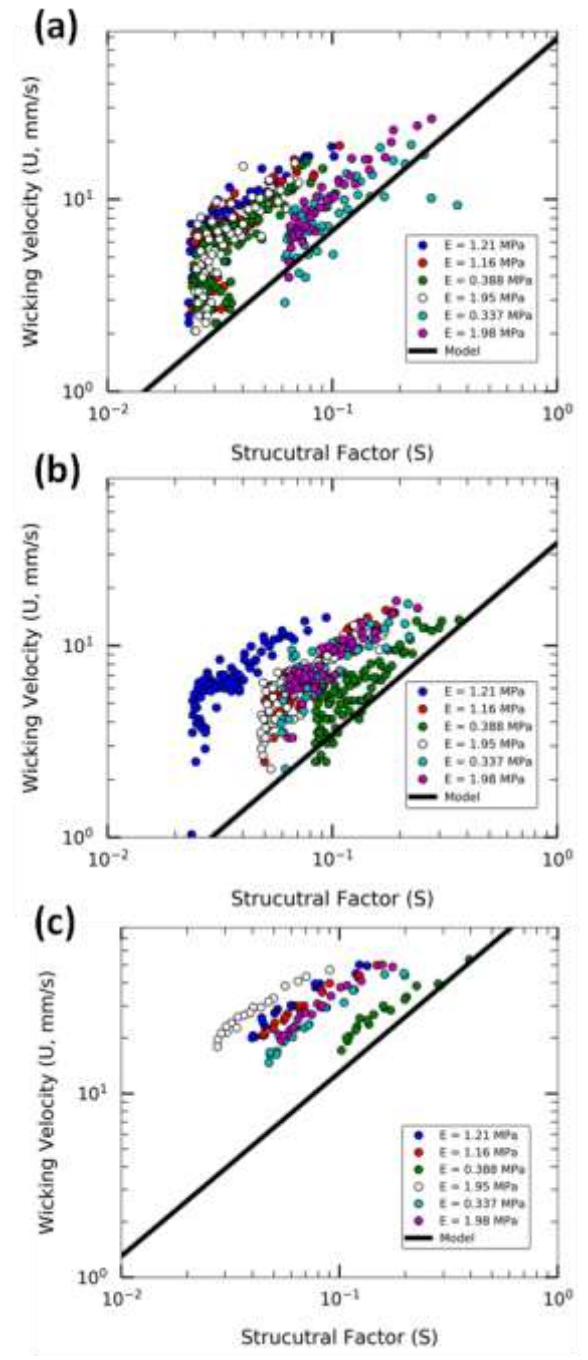


Fig.5 The measured wicking velocities of the samples versus the Structural Factors of the different samples for (a) ethanol (b) isopropyl alcohol (c) isopotane

The aforementioned model for wicking velocity will be used for comparing the measured wicking velocities in this study.

Wicking Velocity Results

Figure 5 displays the wicking velocity results of the PDMS wicking samples for the different working fluids compared to Eqn. (7). These results are based on three trials with the same working fluid. The meniscus extension was obtained through the use of an overhead camera recording the final pillars in the array while the working fluids were evaporating (Resolution =

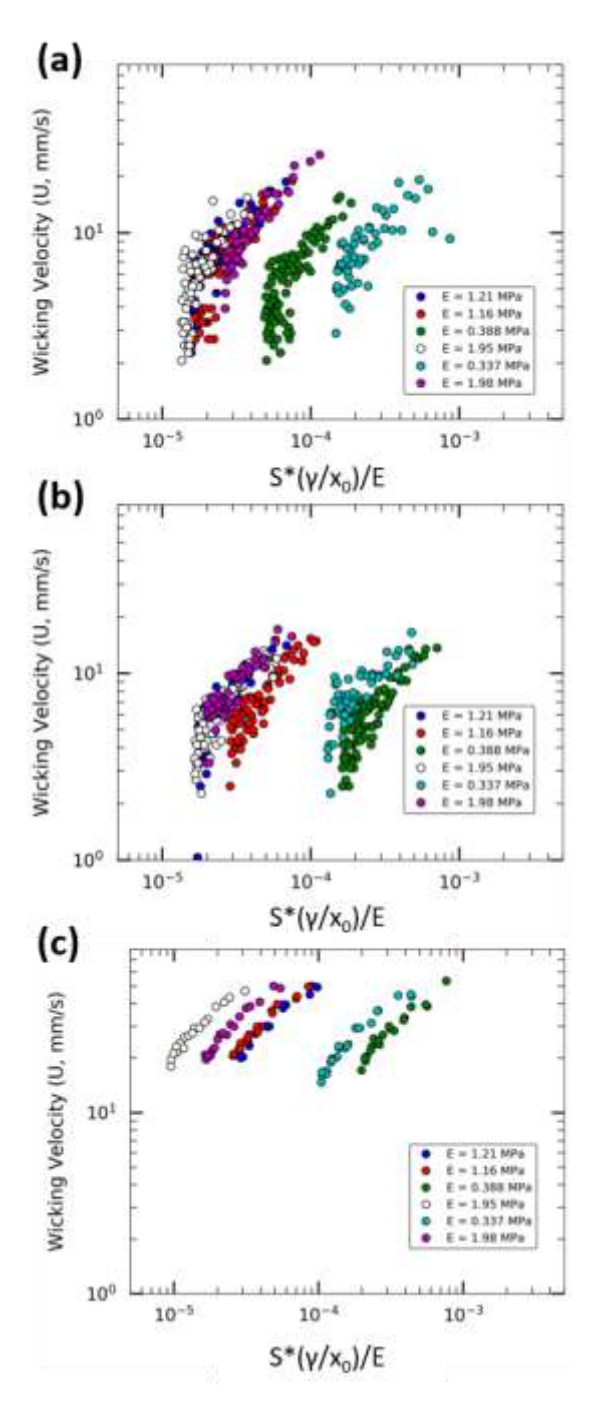


Fig.6 The measured wicking velocities of the samples versus the Structural Factors multipled by the dimensionless property that incorporates the fluid properties, stiffness, and interfacial dynamics for (a) ethanol (b) isopropyl alcohol (c) isooctane

0.176 µm/pixel). For most of the samples tested, the wicking velocity was higher than the given model above a certain S value. However, below a unique S value for both working fluids, the wicking velocity drops from the trend line. This is attributed due to the zippering that begins to occur at a certain length into the wicking array. This drop off is expected due to the increasing amount of drag that occurs that acts on the wetting surface the further the working fluid travels [19].

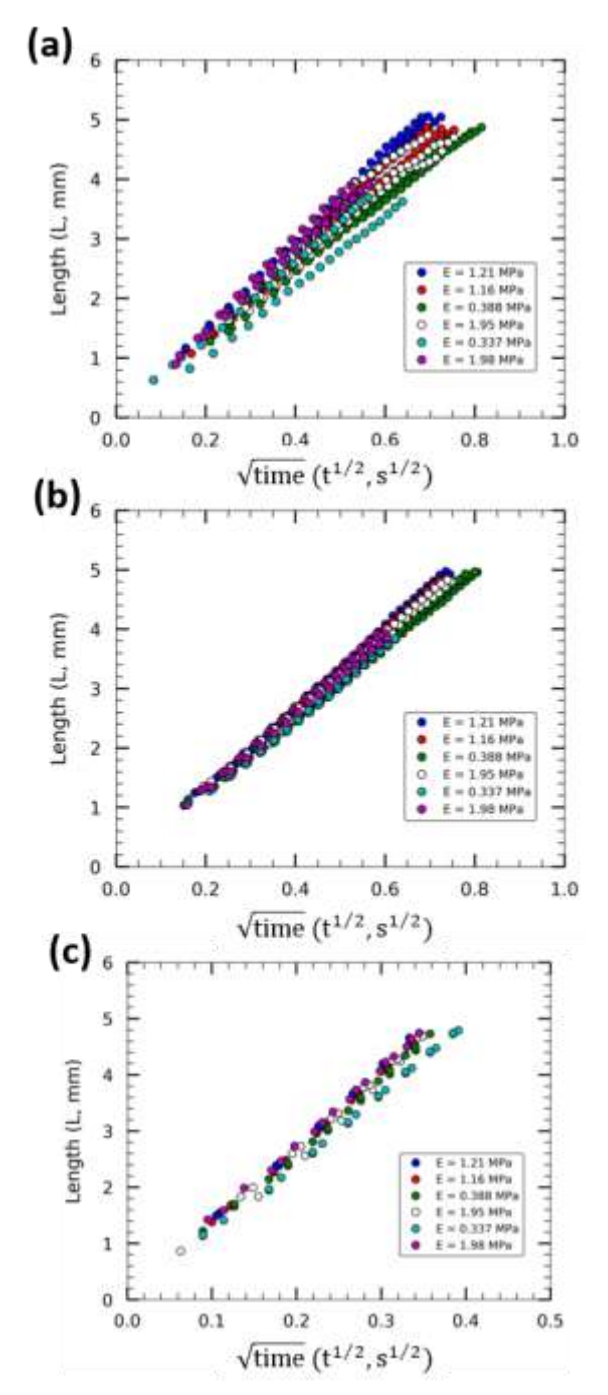


Fig.7 The distance traveled by the working fluids on the different samples as a function of the square root of time for (a) ethanol (b) isopropyl alcohol (c) isooctane

Isooctane does not display this trend since zippering did not occur within the measurement distance.

However, for samples with lower E values (i.e. samples 3 and 6) do exhibit lower wicking velocities than the other samples and falls below the model line. This is true for both regions where zippering occurs or bulk motion occurs. This interesting finding does show that the dynamic motion of the

Table III: The Linear Regression and Statistics for the

Diffusion in Figure 7

Diffusion	in Figure /			
Sample	Working Fluid	$\mathbf{D}^{1/2}$	\mathbb{R}^2	Confidence
				Interval
				(95%)
1	Ethanol	7.227	0.999	0.0162
1	Isopropyl Alcohol	6.692	0.999	0.0140
1	Isooctane	13.66	0.998	0.0564
2	Ethanol	6.764	0.999	0.0109
2	Isopropyl Alcohol	6.634	0.999	0.0095
2	Isooctane	13.44	0.999	0.0421
3	Ethanol	6.167	0.999	0.0201
3	Isopropyl Alcohol	6.245	0.999	0.0060
3	Isooctane	13.03	0.998	0.0424
4	Ethanol	6.637	0.994	0.0454
4	Isopropyl Alcohol	6.493	0.999	0.0119
4	Isooctane	13.41	0.999	0.0354
5	Ethanol	6.364	0.998	0.0145
5	Isopropyl Alcohol	6.169	0.997	0.0854
5	Isooctane	12.23	0.999	0.0262
6	Ethanol	7.303	0.999	0.0131
6	Isopropyl Alcohol	6.545	0.999	0.0061
6	Isooctane	13.75	0.998	0.0237

fluid can create deformations on the surface that can inhibit the locomotion of the fluid. Further experiments will need to be conducted to observe the deformation that occurs on the surface

To gain understanding into the relationship between the wicking velocity and the stiffness of the material, a non dimensional parameter that incorporates the stiffness (E), the fluid properties (y), and the interfacial dynamics (x_0) was created. This parameter was multiplied with S and the velocities were plotted with this new parameter, as shown in Figure 6. Implementing this non dimensional parameter groups together the stiffer samples (i.e. Samples 1, 2, 4, and 6) from the more flexible samples (i.e. Samples 3 and 5). The less stiff samples were also more coupled together. The same drop off in the velocity associated with zippering is also observed with this parameter. This observed grouping is promising in providing more insight into the dynamics of wetting on soft materials, but more experiments will need to be conducted to find a suitable non dimensional parameter to better describe the velocity drop off in more flexible samples.

Diffusion of the Working Fluids in the Pillar Arrays

Along with comparing the wicking velocity with known wicking models, a look at the diffusion of the different fluids through the wicking arrays is presented in this work. It is well documented that the length that the fluid travels through is directly proportional to the square root of time [19]. Figure 7 displays the distance traveled as a function of the square root of time. It can be seen that the relationship for all three working fluids for all six samples is linear, which is what is expected from what is known about diffusion. Another thing that can be noted from the results of these experiments is the repeatability of the experiments. To show the accuracy of the best fit line, the R² and confidence intervals for 95% were calculated. These values are presented in Table III. Based off

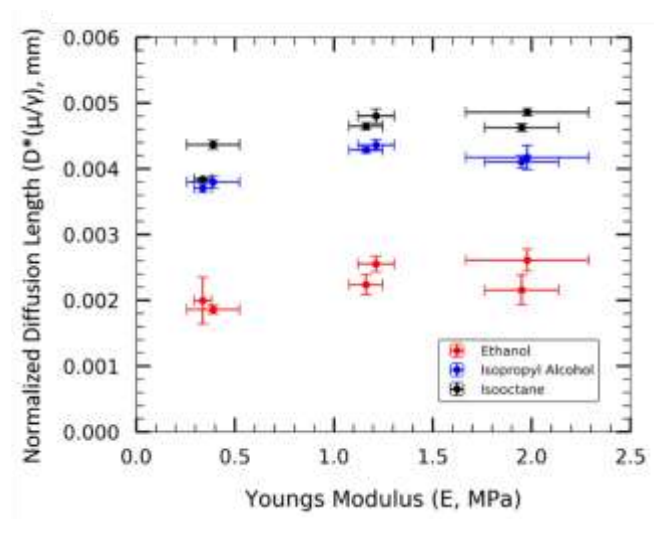


Fig.8 The effective diffusion length as a function of the Young's Modulus of the samples used in this study

of these graphs, the diffusions can be determined through the slopes of the lines. Similar to the results of the wicking velocity, the diffusion for the samples with a lower Young's Modulus is lower than that of the more stiff samples.

To get a further understanding of the change in diffusion as the stiffness decreases, the effective diffusion length, which is defined as the diffusion multiplied by the ratio of the working fluid's dynamic viscosity to its surface tension, is plotted against the Young's Modulus of the sample. This result is displayed in Figure 8. This plot displays a definitive decrease in the diffusion length as the stiffness decreases below 1 MPa. For the other samples above said threshold, the diffusion length is not impacted by the value of the Young's Modulus. This result couples with the velocity results reveals that the deformations that can occur from the wetting dynamics can hinder the motion of a working fluid through the pillar array.

SUMMARY & CONCLUSIONS

This study introduced the impact the stiffness of soft material wicking structures has on the wicking velocity and diffusion of different working fluids. Through analyzing the wicking velocity and diffusion of ethanol, isopropyl alcohol, and isooctane across six PDMS wicking samples of varying stiffness, the wicking performance is affected once the Young's Modulus of a sample is below 1 MPa. Further investigation with materials of lower stiffnesses will provide further insight to the amount of diffusion degradation that occurs due to the deformation of the soft materials. The additional information gathered from future studies can assist in implementing a new wicking velocity model which incorporates the Young's Modulus of a soft material. The information displayed leads to a need to further understand wicking dynamics on soft materials to incorporate wicking applications.

Acknowledgments

This material is based on research partially sponsored by the U.S. Office of Naval Research under Grant No. N00014-15-1-2481. The views and conclusions contained herein are those of the authors and should not be interpreted as necessarily representing the official policies or endorsements, either expressed or implied, of U.S. Office of Naval Research or the U.S. Government.

References

- [1] B.S. Kim et al., "Interfacial wicking dynamics and its impact on critical heat flux boiling heat transfer." pp. Phys. Lett., vol 105, 191601, Nov. 2014.
- [2] G. McHale et al., "Dynamic wetting and spreading and the role of topography," J. Phys.: Condens. Matter, vol. 21, 464122, Oct. 2009.
- [3] Y. Zhu, et al., "Prediction and characterization of dry out heat flux in micropillar wick structures," Langmuir, vol. 7, pp. 1920-1927, Jan. 2016.
- [4] M.B. Mikkelson et al., Controlled deposition of sol-gel sensor material using hemiwicking," J. Micromech. Microeng., vol. 21, 115008, Aug. 2011.
- [5] B.S. Kim et al., "Surface roughening for hemi-wicking and its impact on convective boiling heat transfer," International Journal of Heat and Mass Transfer, vol. 102, pp. 1100-1107, July 2016.
- [6] C. Ding et al., "Wicking Study of Nanostructured Titania Surfaces for Flat Heat Pipes," NSTI-Nanotech, vol. 3, pp. 223-226, 2009.
- [7] I. Levental at al., "Soft biological materials and their impact on cell function," Soft Matter, vol. 3, pp. 299-306, Sept. 2006.
- [8] M. Geoghegan, "Wetting at polymer surfaces and interfaces," Prog. Polym. Sci., vol. 28, pp. 261-302, Aug. 2002.
- [9] B.J. de Gans, and U.S. Schubery, "Inkjet printing of well-defined polymer dots and arrays," Langmuir, vol. 2, pp. 7789-7793, July 2004.
- [1] S.J. Park et al., "Visualization of asymmetric wetting ridges on soft solids with X-ray microscopy," Nature Communications, vol. 5:4369, 10.1038, July 2014.
- [11] R.W. Style et al., "Universal Deformation of Soft Substrates Near a Contact Line and the Direct Measurement of Solid Surface Stresses," Physical Review Letters, vol. 110, 066103, Feb. 2013.
- [12] Z. Cao et al., "dhesion and Wetting of Nanoparticles on Soft Surfaces," Macromolecules, vol. 47, pp. 32 3-3209, April 2014.
- [13] L. Chen et al., "Short time wetting dynamics on soft surfaces," Soft Matter, vol. 7, pp. 9 84-9089, July 2011.
- [14] C. Oshman et al., "Flat flexible polymer heat pipes," J. Micromech. Microeng., vol. 23, 015001, Nov. 2012.
- [15] C. Yang et al., "Flexible heat pipes with integrated bioinspired design," Progress in Natural Science: Materials International, vol. 25, pp. 51-57, Feb. 2015.
- [16] T. Germain et al., "Scalable Stamp Printing and Fabrication of Hemiwicking Surfaces," J. Vis. Exp., vol. 142, e58545, Dec. 2018.
- [17] K. Khanafer et al., "Effects of strain rate, mixing ratio, and stress-strain definition on the mechanical behavior of the polydimethylsiloxane (PDMS) material as related to its biological application," Biomed Microdevices, vol. 11, pp. 503-508, Dec. 2008.

- [18] M. Liu et al., "Influences of heating temperature on mechanical properties of polydimethylsiloxane," Sensors and Actuators A, vol. 151, pp. 42-45, Feb. 2009
- [19] J. Kim et al., "Dynamics of hemiwicking," J. Fluid Mech., vol. 800, pp. 57-71, Aug. 2016.0
 [2] S.R. Krishnan et al., "simple analytic model for
- [2] S.R. Krishnan et al., "simple analytic model for predicting the wicking velocity in micropillar arrays," Scientific Reports, vol. 9, 20074, Dec. 2019